Journal of Power Sources 414 (2019) 412–419

Contents lists available at ScienceDirect

Journal of Power Sources

journal homepage: www.elsevier.com/locate/jpowsour

A Li-Li_2S_4 battery with improved discharge capacity and cycle life at low electrolyte/sulfur ratios

Chao Shen[a,c], Jianxin Xie[b,d], Mei Zhang[b,d], Petru Andrei[a,c], Jim P. Zheng[a,c,e,*], Mary Hendrickson[f], Edward J. Plichta[f]

[a] Department of Electrical and Computer Engineering, Florida A&M University and Florida State University, Tallahassee, FL, 32310, USA
[b] Department of Industrial and Manufacturing Engineering, Florida A&M University and Florida State University, Tallahassee, FL, 32310, USA
[c] Aero-Propulsion, Mechatronics and Energy Center, Florida State University, Tallahassee, FL, 32310, USA
[d] High Performance Materials Institute, Florida State University, Tallahassee, FL, 32310, USA
[e] Center for Advanced Power Systems, Florida State University, Tallahassee, FL, 32310, USA
[f] Army Power Division, RDER-CCA, 5100 Magazine Road, Aberdeen Proving Ground, MD, 21005, USA

HIGHLIGHTS

- Lithium polysulfide electrochemical reactions are restricted by its solubility.
- Li_2S_4 as cathode is not limited by the electrolyte.
- Theoretical specific energy of Li_2S_4 batteries is given.

ARTICLE INFO

Keywords:
Lithium–sulfur batteries
Lithium polysulfide solubility
Li-Li2S4
Electrolyte/sulfur ratio
Discharge capacity

ABSTRACT

Lithium sulfur (Li-S) batteries are promising candidates to replace lithium ion batteries as the next-generation energy storage devices. However, the operation of conventional Li-S batteries at low electrolyte/sulfur ratios is rather challenging with many obstacles to be addressed. In this work we use solid-state Li_2S_4 as the cathode active material to construct a new type of Li-Li_2S_4 battery. With the aid of electrochemical impedance spectrum, we find that the use of $Li_2S_{4(S)}$ in the cathode alleviates the issue of surface coverage encountered under the lean electrolyte condition. We also find that the discharge capacity is not determined by the solubility of Li_2S_4 on the lower plateau of discharge. Consequently, the Li-Li_2S_4 cell with a high sulfur content of 84% and a low E/S ratio of 4.4 ml g^{-1} delivered a much higher discharge capacity compared to a conventional Li-S cell. In addition, improved cycle retention was achieved when controlling the Li-Li_2S_4 cell cycling between Li_2S_4 and Li_2S. We believe that the reported results open a new direction of cathode development for high energy density Li-S batteries.

1. Introduction

Rechargeable lithium-sulfur (Li-S) batteries with a theoretical specific energy of 2500 Wh kg^{-1} (3–5 folds higher than that of Li-ion batteries), are promising candidates to replace Li-ion batteries in many applications [1]. Even though Li-S batteries possess a high theoretical specific energy, several major technical challenges must be overcome to achieve their potential. Many of these challenges are closely related to the formation of soluble lithium polysulfide (LiPS) intermediates. For instance, the irreversible redistribution of LiPS inside the battery leads to degradation of sulfur cathodes and passivation of Li metal anode. The uncontrolled relocation of LiPS further leads to severe active material loss during long-term cycles.

Ultimately, the most critical question to answer in the case of Li-S batteries is whether their high theoretical energy density can be practically delivered. The practical specific energy depends strongly on the electrolyte/sulfur (E/S in ml g^{-1}) ratio of these batteries. To increase the energy density of rechargeable Li-S batteries, the E/S ratio should be decreased as much as possible [2–5]. However, when the E/S ratio is decreased, multiple issues arise that degrade battery performance including discharge capacity, cycle life, and rate capability [6–12]. For instance, Fan et al. [11,13] found that the viscosity of the electrolyte

* Corresponding author. Department of Electrical and Computer Engineering, Florida A&M University and Florida State University, Tallahassee, FL, 32310, USA.
E-mail address: zheng@eng.famu.fsu.edu (J.P. Zheng).

https://doi.org/10.1016/j.jpowsour.2019.01.029
Received 29 October 2018; Received in revised form 26 December 2018; Accepted 12 January 2019
0378-7753/ © 2019 Published by Elsevier B.V.

increases and the reaction rates decrease when the concentration of LiPS is increasing, which results in significantly slower electrodeposition with island nucleation and growth rates up to 75% less than those at low concentrations. In a recent study, our group found that, once the electrolyte becomes saturated with liquid phase high-order LiPS, the solid phase LiPS becomes electrochemically unable for further reduction at normal discharge rates [14,15]. Therefore, the finite solubility of high-order LiPS can potentially lower the specific energy of Li-S batteries to less than 500 Wh kg^{-1}, making them commercially less attractive. These deficiencies need to be addressed urgently in order to be able to operate Li-S batteries at low E/S ratios.

In this work we use solid-state lower-order LiPS, i.e. $Li_2S_{4(S)}$, as the cathode active material to construct a new type of Li-Li_2S_4 battery, which circumvents many of the above deficiencies of conventional Li-S batteries. Li_2S_4 is located at the end of liquid–liquid phase transition chain (Li_2S_8-Li_2S_6-Li_2S_4). Unlike the reduction of Li_2S_8 and Li_2S_6, the reduction of Li_2S_4 involves a single liquid-solid phase transition (simplified as Li_2S_4 to Li_2S) in which the reaction product no longer exists in liquid phase. In this sense, the active material in the electrolyte is progressively consumed, allowing for a continuous dissolution of $Li_2S_{4(S)}$ into the electrolyte. Therefore, by replacing the elemental sulfur with $Li_2S_{4(S)}$ in the cathode, we avoid the solubility limitation encountered on the upper plateau of the discharge in Li-S batteries in which the active material is elemental sulfur. In addition, the cycleability of Li-Li_2S_4 cell is also enhanced because it uses a lower cut-off recharge voltage during cycling to avoid the liquid-solid transformation at the end of charge. We believe this work opens a new direction of cathode development for high energy density Li-S batteries.

2. Experimental

Sulfur,1,2-dimethoxyethane (DME), 1,3-dioxolane (DOL), bis(trifluoromethane)sulfonimide (LiTFSI), and $LiNO_3$ were purchased from Sigma-Aldrich. Lithium sulfide was purchased from Alfa Aesar. Anhydrous ethanol was purchased from VWR.

The synthesized carbon nanotube (CNT) foams contained CNTs (General Nano) with an average diameter of 10 nm and a length of 2 mm, which were assembled in a freestanding three-dimensional conductive network using the method presented in previous papers [14,16]. The obtained foams had a thickness of 100 μm and a density of 125 mg cm^{-3}.

The C/$Li_2S_{4(S)}$ cathodes were made by loading CNT foam with solid-state Li_2S_4. To prepare the Li_2S_4 catholyte, we mixed Li_2S and S powders in a stoichiometric ratio of 1:3 in DME and DOL (1:1 v:v) solution. The Li_2S_4 catholyte was obtained by vigorous magnetic stirring at 45 °C until the two powders were fully dissolved. CNT foams were soaked in the Li_2S_4 catholyte with controlled volume and then dried overnight inside an argon-filled glovebox (MBraun) to evaporate the solvent and obtain C/$Li_2S_{4(S)}$ cathodes with desired loading. The C/S cathodes were made by infiltrating sulfur into the CNT foams via the melt diffusion method. Sulfur powder was placed on the surface of the CNT foam uniformly and then heated and melted into the CNT foam with a hot plate at 158 °C. The C/Li_2S cathodes were prepared by a solution based method [17]. Li_2S powder was dissolved in anhydrous ethanol in a glovebox environment to obtain a 0.5 M Li_2S solution. The CNT foam was first soaked in the solution and then dried overnight until a maximum sulfide loading was achieved.

The electrolyte used during the coin cell assembly was composed of 0.5 M LiTFSI and 0.5 M $LiNO_3$ in DME:DOL (1:1 v:v). The as-prepared cathode was assembled with a piece of Celgard 2400 separator and a Li foil anode (MTI) into a CR2032-type coin cell. 35 μl of electrolyte was added in each cell. The E/S ratios of the cells were computed as the ratio of electrolyte volume in mL to the weight of sulfur element in g in the cathode. In the case of the Li-Li_2S_4 cathode, the weight of sulfur was calculated as $\frac{32\times4}{32\times4+7\times2}\times M_{Li_2S_4}$, where $M_{Li_2S_4}$ is the weight of loaded Li_2S_4 in the cathode.

The galvanostatic cycling measurements were performed on a Neware multichannel battery cycler at a current density of 0.4 mA cm^{-2} at room temperature. The electrochemical impedance spectrum (EIS) of the cells was recorded over a frequency range from 1-10^5 Hz using a Gamry Instruments (Reference 3000) with an AC voltage amplitude of 10 mV at the open circuit potential. The resulting spectrum was analyzed by using Gamry Echem Analyst software.

To characterize the morphology of the cathodes before and after cycling, we performed scanning electron microscopy (SEM) and electron dispersive X-ray spectroscopy (EDS) using a JEOL microscope (JSM7401F) at a beam voltage of 10 kV and 20 kV, respectively. To characterize the cathodes after full discharge, the disassembled cathodes were washed with DOL solution five times to remove the soluble polysulfides and Li salt after cycling and, then, left in the glove box overnight to evaporate the remaining solvent. The UV-vis spectroscopy of Li_2S_4 solution was measured in a sealed quartz glass cuvette (VWR) with a path length of 10 mm using a UV-vis-NIR spectrophotometer (Varian Cary 5000) in a range of wavelengths spanning from 300 to 800 nm. The X-ray photoelectron spectroscopy (XPS) spectrum of Li_2S_4 was obtained using a PHI-5000C ESCA system (Perkin Elmer) with MgKα radiation (1253.6 ev).

3. Results and discussion

The discharge capacity of conventional Li-S batteries is highly dependent on the E/S ratio as reported in many papers [2,11,18,19]. Fig. 1 plots the voltage profiles of Li-S cells with C/S cathodes at different E/S ratios. Here a fixed electrolyte volume (35 μl) was added in each cell to ensure identical electrolyte wetting conditions and the sulfur loading was varied to obtain different E/S ratios. As expected, all the measured voltage profiles present two discharge plateaus: an upper plateau representing the reduction from sulfur to Li_2S_4 and a lower plateau representing the conversion from Li_2S_4 to Li_2S. The Q_2/Q_1 ratio of the lower plateau capacity (Q_2) to the upper plateau capacity (Q_1) exhibits a sharp drop when decreasing the E/S ratio. When the E/S ratio is relatively high (e.g., 17.5 ml g^{-1}), both Q_1 and Q_2/Q_1 are close to the theoretical values of 418 mAh g^{-1} and 3, respectively, indicating that most sulfur is fully reduced to Li_2S_4 and that most Li_2S_4 can be further reduced to Li_2S. Ratio Q_2/Q_1 decreases to as low as 0.4 when the E/S ratio decreases to 4.4 ml g^{-1}. A similar phenomenon was also observed by other groups [19,20].

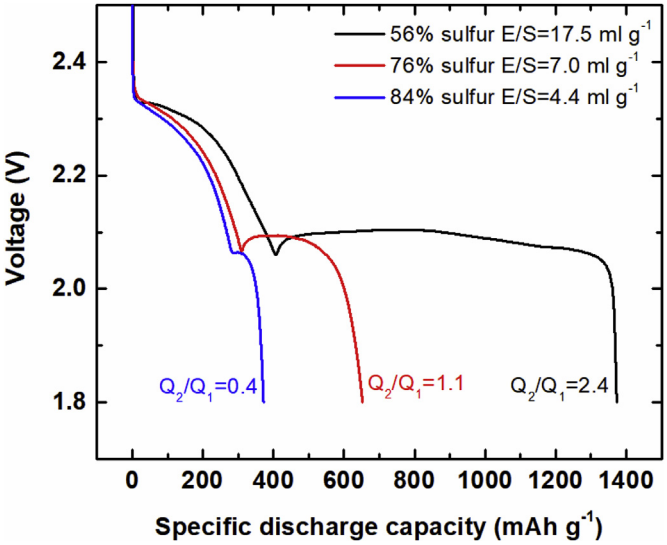

Fig. 1. Discharge profiles of Li-S cells with C/S cathodes and the corresponding Q_2/Q_1 ratios.

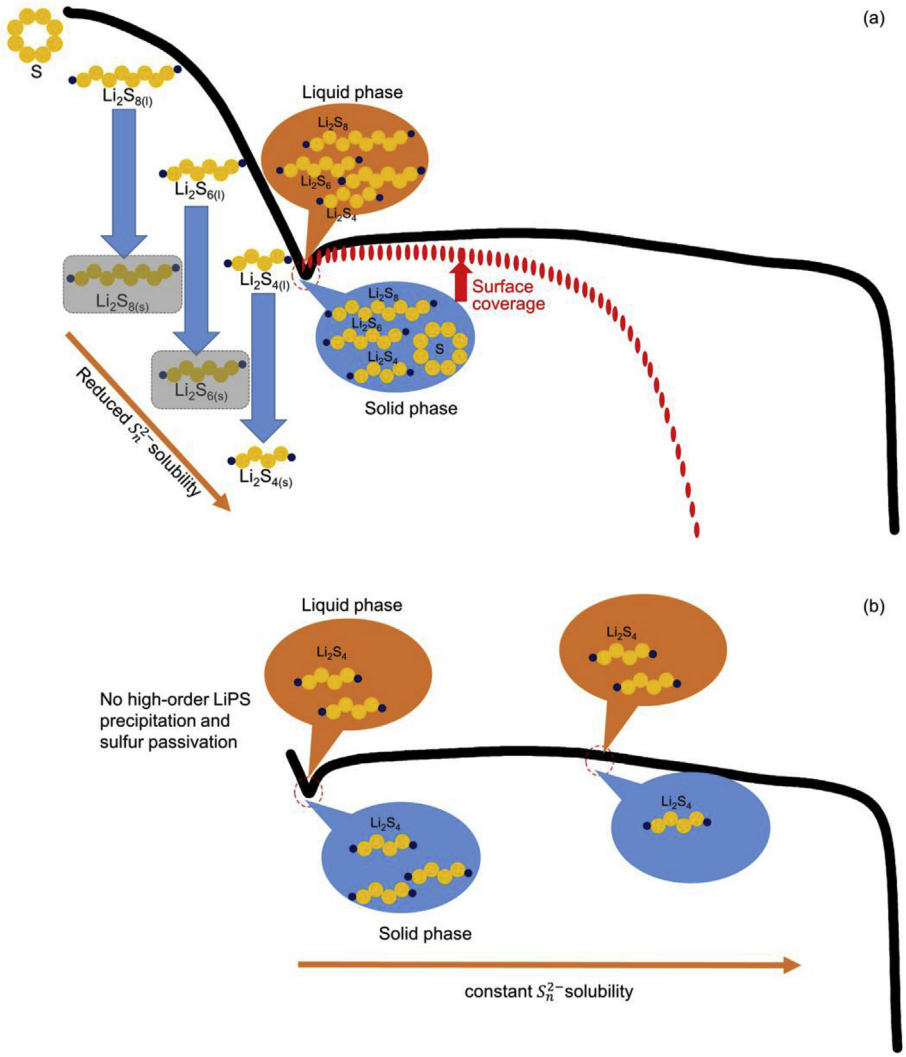

Fig. 2. Comparative illustration of the discharge processes in (a) Li-S and (b) Li-Li_2S_4 cells.

There are multiple reasons that can account for this phenomenon, as illustrated in Fig. 2a. These reasons are in general attributed to the premature formation of insoluble solid products and surface passivation in the cathode. First, the solubility limit of LiPS can be easily reached at low E/S ratios resulting in a fast formation of solid LiPS. As shown both experimentally [14,15] and theoretically [21], the precipitated high-order LiPS exhibits ultralow redox activities, becoming a "dead" residual in the battery. Second, as apparent from Fig. 1, not all the solid sulfur is fully dissolved and reduced in the electrolyte at the end of the upper plateau, which suggests that part of the cathode surface might remain electrochemically inactive on the lower plateau. Finally, as it was recently reported in the literature, locally distributed solid sulfur precipitation through disproportionation reactions can cause an increase of the interfacial resistance under lean electrolyte conditions [22], resulting again in a decrease of the specific capacity. Consequently, the residual $LiPS_{(S)}$ and sulfur in the cathode will occupy a significant fraction of active surface, for which reason the cathode will become passivated quickly once the solid products start depositing.

To address the capacity limitation caused by the finite LiPS solubility on the upper plateau and enhance the utilization of active material, we propose a new type of Li-Li_2S_4 battery, which uses solid-state Li_2S_4 as the active material in the cathode. The proposed cell configuration avoids the negative effects associated with high-order LiPS. For instance, since the electrolyte contains mostly dissolved Li_2S_4 molecules, which are expected to have a larger mobility than the higher-order LiPS molecules (because of the reduced size of Li_2S_4 molecules), the active material is expected to diffuse easier to the cathode surface and participate in electrochemical reactions. The $Li_2S_{4(S)}$ dissolves continuously in the electrolyte during the discharge of the battery (see Fig. 2b) and the battery does not suffer from the negative effects attributed to the additional precipitation of Li_2S_4, like in the case of conventional Li-S batteries.

In Figs. S1 and S2 in Supplementary Material we present the results of UV-vis spectrum of Li_2S_4 solution and XPS spectrum of solid-state Li_2S_4, respectively. The UV-vis spectrum shows a large absorption peak at 420 nm, which is attributed to s_4^{2-} [23]. The XPS spectrum shows two pairs of S doublets, correspond to terminal sulfur atoms (S^T) and the bridging sulfur atoms (S^B) in the chain structure of Li_2S_4, respectively. The quantitative analysis shows that the atom ratio of terminal/bridging sulfur is ca. 1.06, which is close to the theoretical value of 1 for Li_2S_4 molecule [24,25]. The above result confirms that the major species in the synthesized polysulfide is indeed Li_2S_4.

Fig. 3 presents the SEM images of the CNT foam before and after S/Li_2S_4 infiltration. As seen in Fig. 3a, in the pristine CNT foam, the CNTs are randomly entangled together and the cathode has a high porosity. The morphologies of the C/S (see Fig. 3b) and C/$Li_2S_{4(S)}$ cathode (see Fig. 3c) are relatively similar to each other and the active materials are evenly distributed and form a relatively uniform coating on the surface of CNTs. The cathodes still possess a sufficient number of nanopores and mesopores to allow for the electrolyte penetration during cell

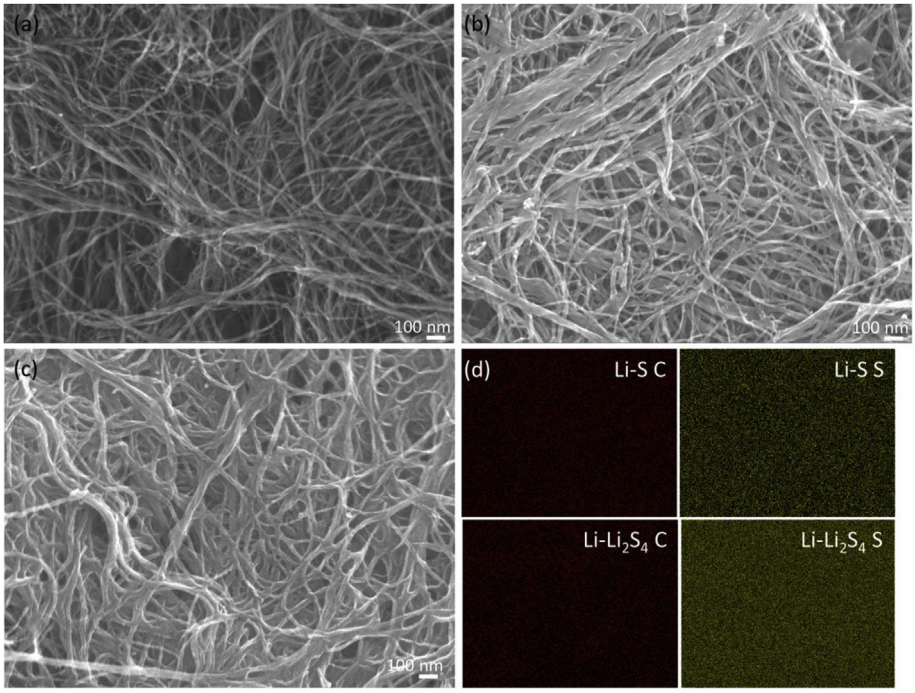

Fig. 3. Morphology of the CNT cathode before and after S/Li_2S_4 infiltration: (a) SEM image of the pristine CNT foam. (b) SEM image of the C/S cathode. (c) SEM image of the C/$Li_2S_{4(S)}$ cathode. (d) EDX mapping of the SEM images shown in (b) and (c).

operation. The EDS mapping results shown in Fig. 3d indicate that sulfur is indeed distributed more or less uniformly inside the cathode.

The CNT foam used is our work has many characteristics suitable to function as a sulfur host. First, the excellent electron transport properties of individual CNTs and the effective crosslinks between CNTs result in a high electrical conductivity of the cathode. The high surface area given by the high density of nano-scale pores provides abundant active sites for electrochemical reactions. The large void volume can accommodate the volume expansion during the lithiation process and the freestanding architecture eliminates the stability issues related to binder decomposition during cell operation. Finally, the three-dimensional and freestanding CNT network promotes efficient access to electrolyte, which is particularly important at low E/S ratios.

The Li-S and Li-Li_2S_4 cells with the same initial sulfur content of 84% and E/S ratio of 4.4 ml g^{-1} are discharged under a current density of 0.4 mA cm^{-2}, which is repeatedly interrupted at different states of discharge to measure the EIS curves (see Fig. 4a). The above sulfur content and E/S ratio is adequate for practical applications [26–28]. In addition, the E/S ratio used in our cells is well below the value imposed by the solubility limit of Li_2S_4 (ca. 16 ml g^{-1}). The small portion of discharge capacity in the upper plateau is attributed to the disproportionation reactions of LiPS [29–31]. More importantly, despite having a much smaller capacity on the upper plateau and accordingly a lower theoretical capacity (1254 mAh g^{-1} vs. 1672 mAh g^{-1}), in the first cycle the Li-Li_2S_4 cell still has a much higher discharge capacity than the Li-S cell (536 mAh g^{-1} vs. 392 mAh g^{-1}).

Fig. 4b–c presents the EIS curves of the Li-S cell and Li-Li_2S_4 cell at selected states of discharge. These spectra are fitted to the two equivalent circuits introduced by Kolosnitsyn et al. [32], represented in the inset of Fig. 4d. The two circuits (circuits I and II) correspond to fully charged/discharged cells (points A, D in Li-S cell and point D in Li-Li_2S_4 cell) and to partially charged/discharged cells (points B-C in Li-S cell and point B-D in Li-Li_2S_4 cell), respectively. In the equivalent circuits, R_0 represents the ohmic resistance contribution resulting from the electrolyte resistance, current collectors, and cell connections, R_1 represents the combined interfacial resistance on cathode and anode, and R_2 represents the charge transfer resistance [32–36]. At different state of discharge, the variation of R_0 is normally associated with electrolyte properties such as chemical composition or viscosity, while R_2 is closely related to cathode surface coverage condition by the solid products.

The fitting results are presented in Fig. 4d at different depths of discharge. The larger values of R_1 and R_2 at point A can be attributed to the more insulating nature of elemental sulfur than $Li_2S_{4(S)}$. The value of R_0 is higher in the case of the Li-Li_2S_4 cell because the $Li_2S_{4(S)}$ dissolves quickly and saturates the electrolyte, increasing the electrolyte viscosity, upon cell assembly. At point B, where the cell was discharged to 2.1 V, the concentration of LiPS in Li-S cell reaches a maxima [32,35–37] and, as a result, R_0 increases from 5.9 Ω to 17.5 Ω and remains relatively constant afterwards. It is also likely that the accumulation of LiPS precipitates in the separator can contribute to this resistance change. The pileup of LiPS at this state of discharge not only increases the internal resistance but also blocks the subsequent reaction pathway. On the contrary, R_0 does not change much in the case of the Li-Li_2S_4 cell the electrolyte is saturated with Li_2S_4, which has a constant and relatively low solubility. Therefore, the viscosity of the electrolyte in the Li-Li_2S_4 cell remains lower to favor the subsequent electrochemical reactions. In addition, R_1 and R_2 decrease in both Li-S and Li-Li_2S_4 cell due to the dissolution of sulfur and $Li_2S_{4(S)}$, respectively.

At point C, resistance R_2 shows distinct trends in the two cells: R_2 starts to increase in the Li-S cell, indicating that the active surface is gradually covered with insulating Li_2S and it decreases in the Li-Li_2S_4 cell, probably due to the further consumption of $Li_2S_{4(S)}$. At point D, R_2 exhibits a dramatic increase due to the accumulation of Li_2S, which fully covers the active surface and terminates the reduction reaction prematurely in both cells. Interestingly, although the Li-S cell delivers a lower discharge capacity, it possesses a much higher R_2 (398.4 Ω vs. 88.2 Ω) compared with the Li-Li_2S_4 cell. In addition, a sharper voltage drop is observed at the end of discharge in the Li-S cell. The above results indicate that the effective surface area for the reduction reaction is smaller in the Li-S cell that in the Li-Li_2S_4 cell, while charge transfer is improved during the electrochemical deposition of Li_2S, increasing the duration of the discharge in the Li-Li_2S_4 cell.

The long-term cycle performance of the Li-Li_2S_4 cell is compared with that of the Li-S cell in Fig. 5. In order to restrict the Li-Li_2S_4 cell to

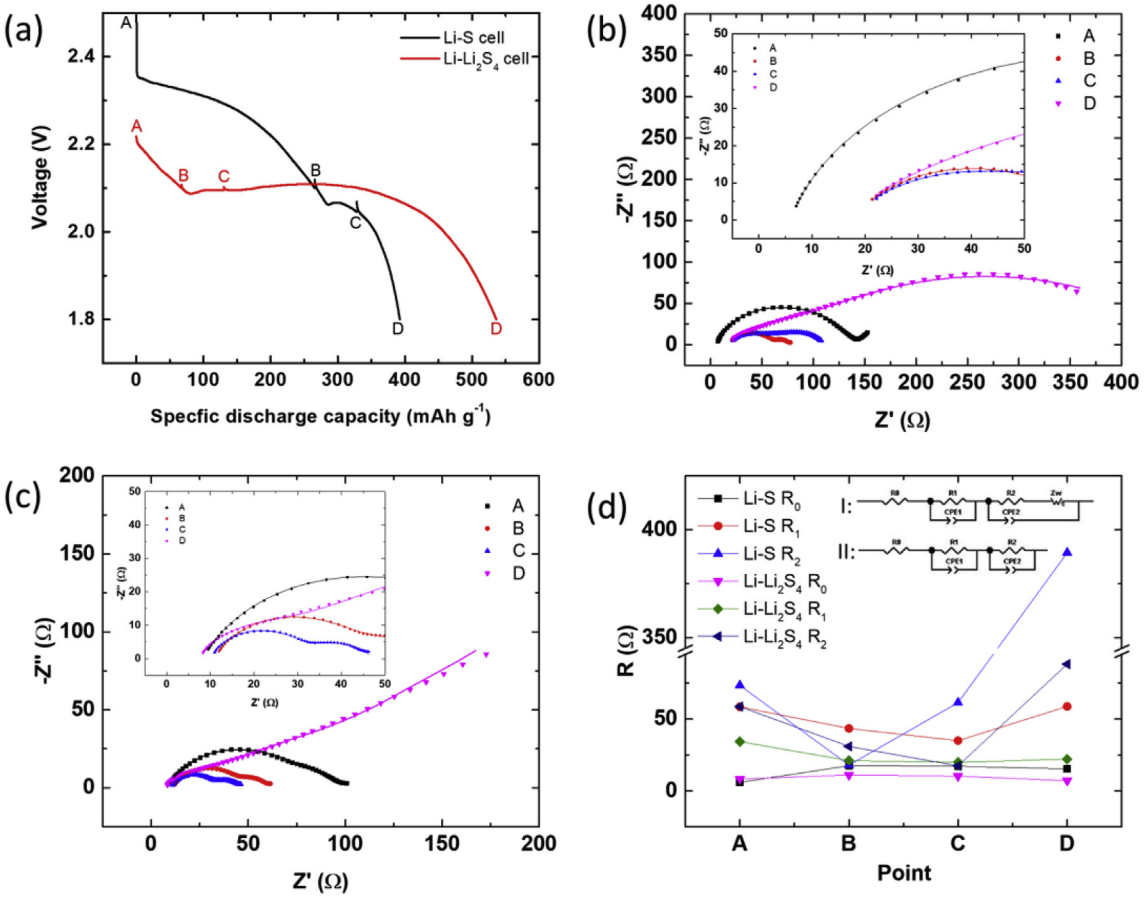

Fig. 4. Discharge profiles at a current density of 0.4 mA cm^{-1} and EIS measurements of the Li-S and Li-Li_2S_4 cells: (a) discharge profiles of the Li-S and Li-Li_2S_4 cells; (b) EIS spectra of the Li-S cell; (c) EIS spectra of the Li-Li_2S_4 cell (the experimental values of the EIS are denoted with symbols); (d) fitting result of EIS spectra of the Li-S and Li-Li_2S_4 cells.

cycle within the lower plateau, a lower cut-off voltage for recharge (2.35 V vs. 2.8 V) was selected. The voltage profiles of the Li-Li_2S_4 cell are compared with those of the Li-S cell in Fig. 5a–b. It is worth mentioning that the obtained Q_2 for Li-Li_2S_4 cell is higher than the value imposed by the solubility limitation (ca. 401.3 mAh g^{-1}), which again indicates that, in the case of Li-Li_2S_4 battery, the solubility of Li_2S_4 does not represent an intrinsic limitation due to the continuous dissolution of $Li_2S_{4(S)}$ in the electrolyte. It is important to note that, in the following cycles, the Q_2/Q_1 ratio shows a slightly increasing trend (see Fig. 5b), which suggests that a small fraction of high-order LiPS was in fact formed at the selected cut-off voltage.

In addition to the lower initial capacity, conventional Li-S cell suffers from a significant capacity loss during the 2nd cycle, which reduces their rechargeable capacity drastically. This phenomenon was also observed and reported in the literature with high and medium E/S ratios by other research groups [38–40]. The capacity loss in our Li-S cells is due to the incomplete conversion during the charge process, which is suggested by the decrease of capacity Q_1 from the 1st to the 2nd cycle in Fig. 5a and by the extremely high initial Coulombic efficiency of 170% (note that we define the Coulombic efficiency as the ratio of the specific discharge capacity to the specific charge capacity in the same cycle; for instance, the specific discharge and charge capacity are 378.1 and 222.3 mAh g^{-1}, respectively, which results in an initial Coulombic efficiency of 170%). On the contrary, the Li-Li_2S_4 cell proposed in this work does not suffer from a significant decay of the capacity during the initial cycles since it does not involve the liquid-to-solid phase transformation at the end of charge. Instead, our Li-Li_2S_4 cells exhibit some fluctuations of the discharge capacity during the initial cycles, which can be related to the redistribution of Li_2S_4 and Li_2S in the conductive matrix. It maintains a relatively stable discharge capacity during the following cycles, although a gradual capacity fade over cycles is still observable. Despite a reduced LiPS dissolution, the progressive changes in the morphology of the cathode structure due to the continuous dissolution and crystallization processes as well as the gradual formation of high-order LiPS may still lead to the slow capacity decay of the cell. We also observe some fluctuation of the discharge capacity after 50 cycles, which is most likely due to the random pore blocking and unblocking that can take place under low E/S ratio conditions. In addition, we also compared the rate performance of Li-S and Li-Li_2S_4 cell for current densities ranging from 0.4 mA cm^{-2} to 1.6 mA cm^{-2} and the result is plotted in Fig. 5d. As seen in the figure, the Li-Li_2S_4 cell delivers significantly higher capacities at all the current densities than the Li-S cell, and the capacity can recover to 649.4 mAh g^{-1} when the current density returns to 0.4 mA cm^{-2}. We also notice that the Li-Li_2S_4 cell exhibits a larger capacity drop at large current densities. It is because that the majority of discharge capacity comes from the lower plateau, which involves the solid deposition process. When the discharge current increases, the active surface is being covered faster by the solid product. In the case of Li-S cell, the majority of discharge capacity is contributed from the upper plateau, which refers to the electrochemical reduction in liquid phase with a relatively higher reaction kinetics.

The SEM images in Fig. 6 show the morphologies of C/S and C/$Li_2S_{4(S)}$ cathodes in the fully discharged state after 50 cycles. Note that since the cathodes were washed with DOL solution five times to remove the soluble polysulfides and Li salt, the precipitate seen in the SEM image is solely Li_2S. Distinguishable morphology differences between the two cathodes were observed after 50 cycles. In the case of the C/S cathode, large Li_2S particles can be observed on the CNT surface and

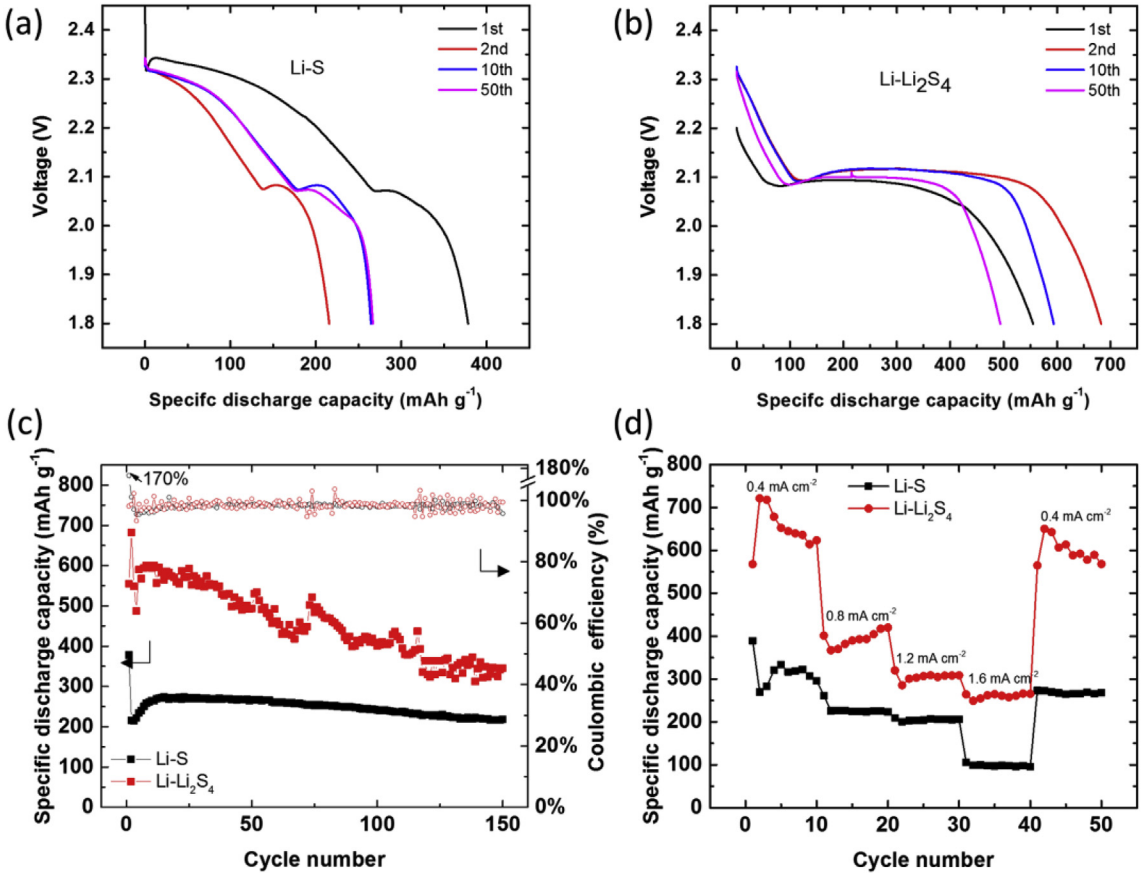

Fig. 5. Electrochemical performance of the Li-S and Li-Li_2S_4 cells: (a) the discharge profiles of the Li-S cell in different cycles at a current density of 0.4 mA cm^{-2}; (b) the discharge profiles of the Li-Li_2S_4 cell in different cycles at a current density of 0.4 mA cm^{-2}; (c) the cycling performance of the Li-S and Li-Li_2S_4 cells at a current density of 0.4 mA cm^{-2}. (d) the rate performance of the Li-S and Li-Li_2S_4 cells for current densities ranging from 0.4 mA cm^{-2} to 1.6 mA cm^{-2}.

the overall deposition is rather non-uniform. In the case of the C/$Li_2S_{4(S)}$ cathode, the volume fraction of the Li_2S deposit is higher, corresponding to a higher discharge capacity. Moreover, despite a higher volume fraction of Li_2S, a more uniform deposition of Li_2S film was observed. Since the deposition and accumulation of nonconductive and insoluble Li_2S films is known to cause structural deterioration of cathodes, a better regulation of Li_2S growth on the cathode surface would facilitate the electronic and ionic pathway for stable cycling especially at low E/S ratios. In Fig. S3 in Supplementary Material we also provide the SEM image of C/S cathode from a Li-S cell with a lower sulfur content (56%) and a higher E/S ratio (17.5 ml g^{-1}). Apparently, the growth of Li_2S is significantly more uniform in this cathode compared to both the cathodes presented in Fig. 6. Therefore, improving the electrodeposition kinetics and promoting a uniform deposition of Li_2S remains a critical challenge for stable cycling of Li-S batteries at low E/S ratios.

Finally, we compare the performance of our Li_2S_4 cathode to the performance of a cathode made with commercial Li_2S. It was found that the sulfur content cannot exceed 75% using the solution-based method [17] and, even with this relatively low loading, the Li-Li_2S cell still suffers from a high initial overpotential, low Coulombic efficiency, and fast cycle decay (see Fig. S4 in Supplementary Material) due to the slow kinetics and the high activation energy caused by the electrically and ionically-insulating nature of Li_2S. The size reduction of Li_2S particle and the better distribution of Li_2S in the cathode are essential to enhance the utilization rate of active material for sulfide cathode. In comparison with S and Li_2S, the utilization of Li_2S_4 is kinetically more favorable due to its dissolution nature.

To further demonstrate the advantage of the Li-Li_2S_4 batteries, the theoretical specific energy of Li-Li_2S_4 batteries is compared with that of

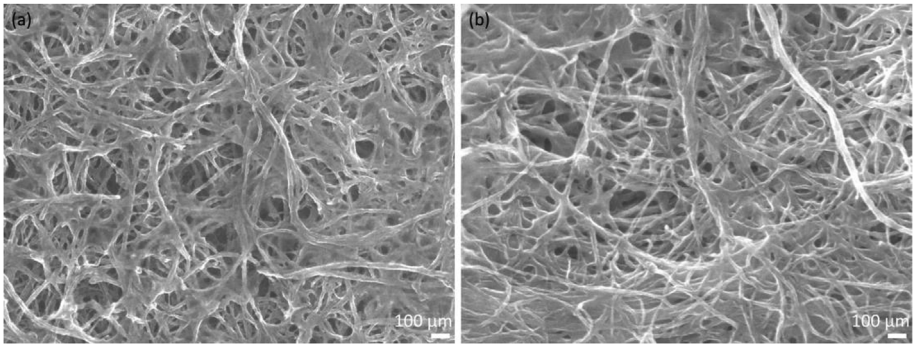

Fig. 6. SEM image of (a) C/S cathode and (b) C/$Li_2S_{4(S)}$ cathode in the fully discharged state after 50 cycles.

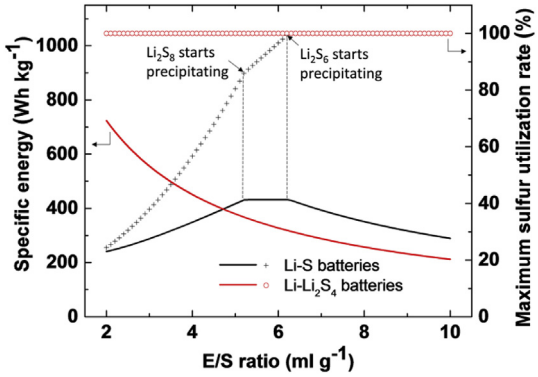

Fig. 7. Theoretical specific energy (continuous line) and maximum sulfur utilization rate (symbols) of Li-S and Li-Li_2S_4 batteries as a function of E/S ratio. The calculations are made by assuming that the LiPS have a finite solubility in the electrolyte and, once this finite solubility is reached, LiPS start precipitating. Due to the low dissolution rate of high-order LiPS in the electrolyte, we assume that the solid high-order LiPS cannot be further reduced and become "unutilized" active material. These assumptions are good for moderate and high discharge rates.

conventional Li-S batteries at various E/S ratios in Fig. 7. The theoretical specific energies are computed by assuming that the density of the electrolyte is 1.1 g ml^{-1} [41] and the solubilities of Li_2S_8, Li_2S_6, and Li_2S_4 in our electrolyte are [S] = 6 M, 5 M, and 2 M [21], respectively. These finite solubilities result in the following values of the E/S ratio required for full dissolution of Li_2S_8, Li_2S_6, and Li_2S_4: 5.2 ml g^{-1}, 6.3 ml g^{-1}, 15.6 ml g^{-1}, respectively. In addition, we also assume that the reduction of S to Li_2S includes the sequential reduction processes from S to Li_2S_8, Li_2S_8 to Li_2S_6, Li_2S_6 to Li_2S_4, and Li_2S_4 to Li_2S and, at sufficiently high discharge rates, the precipitated high-order LiPS does not have enough redox activity to be further reduced and utilized. This phenomenon is observed in a coin cell configuration with the CNT foams as cathode material [14], however, it is expected that at sufficiently high discharge currents, the same effect can also be applied to a pouch cell configuration with different electron conductive materials as cathodes. Finally, we assume that the average discharge voltage is 2.15 V for the Li-S cell and 2.1 V for the Li-Li_2S_4 cell. The detailed process of calculation can be found in the Supplementary Material. It can be seen that, at relatively high E/S ratios, e.g., > 6.3 ml g^{-1}, the conventional Li-S batteries have higher specific energy due to their higher theoretical specific capacity. However, when the E/S ratio is reduced, the maximum sulfur utilization rate decreases as the concentration of higher-order LiPS exceeds the solubility limit and the precipitated LiPS becomes electrochemically inactive for subsequent reactions (see Fig. 2a). Specifically, Li_2S_6 starts depositing when the E/S ratio is less than 6.3 ml g^{-1}, while Li_2S_8 precipitates when the E/S ratio is less than 5.2 ml g^{-1}. In contrast, as we have demonstrated in this study, the utilization of Li_2S_4 is theoretically 100% and is not hindered by its solubility limit even at lower E/S ratios. When the E/S ratio is decreased below 4.7 ml g^{-1}, the higher sulfur utilization eventually compensates the lower theoretical specific capacity for Li-Li_2S_4 batteries. For most practical applications, the operation of batteries at low E/S ratios is a prerequisite and, therefore, the proposed Li-Li_2S_4 system is promising for better utilization of active material.

In this work, we have successfully improved the energy density of Li-S batteries by rationally selecting an alternative cathode active material. Using $Li_2S_{4(S)}$ as the active material and cycling the batteries to form only Li_2S_4 and Li_2S alleviates the negative effects related to the surface coverage when operating the cells under low E/S ratio conditions. Nevertheless, it is worth mentioning that although the performance of Li-Li_2S_4 cells is better that of conventional Li-S cells under the harsh test condition, the obtained discharge capacity in this study is below its theoretical value of 1254 mAh g^{-1}. Therefore, cell components and parameters such as cathode pore structure, sulfur/carbon ratio, electrolyte volume and composition, and cycle scheme can be further optimized to improve the cell performance. In addition, since the active material in Li-Li_2S_4 batteries is a soluble polysulfide, the various recently reported strategies to effectively reduce the diffusion of LiPS molecules towards the anode remain beneficial for improving the cycle performance of these batteries [42–47].

4. Conclusions

In this work we propose to use solid-state Li_2S_4 as the cathode active material to construct a new type of Li-Li_2S_4 battery. By replacing elemental sulfur with Li_2S_4, we avoid the negative effects related to the solubility limit previously encountered on the upper plateau of discharge curves of conventional Li-S batteries. We found that, on the lower plateau of discharge, the discharge capacity is not limited by the solubility of Li_2S_4 and we are able to obtain a much higher discharge capacity in cells with a sulfur content as high as 84% and an E/S ratio as low as 4.4 ml g^{-1}. In addition, we are able to improve the cycle retention of the proposed Li-Li_2S_4 cell by narrowing the cycling voltage window to reduce the capacity loss during the initial cycles. The reported results of Li_2S_4 cathode open a new direction of cathode development for high energy density Li-S batteries.

Acknowledgments

This work was supported by US Army Power Division under contract No. GTS-S-15-014 and by the National Science Foundation under Grant No. 1609860. The authors would also like to acknowledge L. Jin and E. Lochner for conducting and discussing on the XPS test.

Appendix A. Supplementary data

Supplementary data to this article can be found online at https://doi.org/10.1016/j.jpowsour.2019.01.029.

References

[1] J.W. Choi, D. Aurbach, Promise and reality of post-lithium-ion batteries with high energy densities, Nat. Rev. Mater. 1 (2016) 16013, https://doi.org/10.1038/natrevmats.2016.13.
[2] M. Hagen, P. Fanz, J. Tübke, Cell energy density and electrolyte/sulfur ratio in Li-S cells, J. Power Sources 264 (2014) 30–34, https://doi.org/10.1016/j.jpowsour.2014.04.018.
[3] B.D. McCloskey, Attainable gravimetric and volumetric energy density of Li-S and Li ion battery cells with solid separator-protected Li metal anodes, J. Phys. Chem. Lett. 6 (2015) 4581–4588, https://doi.org/10.1021/acs.jpclett.5b01814.
[4] D. Eroglu, K.R. Zavadil, K.G. Gallagher, Critical link between materials chemistry and cell-level design for high energy density and low cost lithium-sulfur transportation battery, J. Electrochem. Soc. 162 (2015) 982–990, https://doi.org/10.1149/2.0611506jes.
[5] X. Yang, X. Li, K. Adair, H. Zhang, X. Sun, Structural design of lithium–sulfur batteries: from fundamental research to practical application, Electrochem. Energy Rev. (2018), https://doi.org/10.1007/s41918-018-0010-3.
[6] H. Schneider, T. Weiß, C. Scordilis-Kelley, J. Maeyer, K. Leitner, H.-J. Peng, R. Schmidt, J. Tomforde, Electrolyte decomposition and gas evolution in a lithium-sulfur cell upon long-term cycling, Electrochim. Acta 243 (2017) 26–32, https://doi.org/10.1016/j.electacta.2017.05.034.
[7] L. Qie, C. Zu, A. Manthiram, A high energy lithium-sulfur battery with ultrahigh-loading lithium polysulfide cathode and its failure mechanism, Adv. Energy Mater. 6 (2016) 1–7, https://doi.org/10.1002/aenm.201502459.
[8] J. Brückner, S. Thieme, H.T. Grossmann, S. Dörfler, H. Althues, S. Kaskel, Lithium-sulfur batteries: influence of C-rate, amount of electrolyte and sulfur loading on cycle performance, J. Power Sources 268 (2014) 82–87, https://doi.org/10.1016/j.jpowsour.2014.05.143 Short communication.
[9] S.S. Zhang, Improved cyclability of liquid electrolyte lithium/sulfur batteries by optimizing electrolyte/sulfur ratio, Energies 5 (2012) 5190–5197, https://doi.org/10.3390/en5125190.
[10] C. Yan, X.B. Cheng, C.Z. Zhao, J.Q. Huang, S.T. Yang, Q. Zhang, Lithium metal protection through in-situ formed solid electrolyte interphase in lithium-sulfur batteries: the role of polysulfides on lithium anode, J. Power Sources 327 (2016) 212–220, https://doi.org/10.1016/j.jpowsour.2016.07.056.
[11] F.Y. Fan, Y.-M. Chiang, Electrodeposition kinetics in Li-S batteries: effects of low electrolyte/sulfur ratios and deposition surface composition, J. Electrochem. Soc.

164 (2017) A917–A922, https://doi.org/10.1149/2.0051706jes.
[12] Z.-W. Zhang, H.-J. Peng, M. Zhao, J.-Q. Huang, Heterogeneous/homogeneous mediators for high-energy-density lithium-sulfur batteries: progress and prospects, Adv. Funct. Mater. 1707536 (2018) 1707536, https://doi.org/10.1002/adfm.201707536.
[13] F.Y. Fan, M.S. Pan, K.C. Lau, R.S. Assary, W.H. Woodford, L.A. Curtiss, W.C. Carter, Y.-M. Chiang, Solvent effects on polysulfide redox kinetics and ionic conductivity in lithium-sulfur batteries, J. Electrochem. Soc. 163 (2016) 3111–3116, https://doi.org/10.1149/2.1181614jes.
[14] C. Shen, J. Xie, M. Zhang, P. Andrei, M. Hendrickson, E.J. Plichta, J.P. Zheng, Understanding the role of lithium polysulfide solubility in limiting lithium-sulfur cell capacity, Electrochim. Acta 248 (2017) 90–97, https://doi.org/10.1016/j.electacta.2017.07.123.
[15] C. Shen, J. Xie, M. Zhang, J.P. Zheng, M. Hendrickson, E.J. Plichta, Communication—effect of lithium polysulfide solubility on capacity of lithium-sulfur cells, J. Electrochem. Soc. 164 (2017) A1220–A1222, https://doi.org/10.1149/2.1381706jes.
[16] C. Shen, J. Xie, T. Liu, M. Zhang, P. Andrei, L. Dong, M. Hendrickson, E.J. Plichta, J.P. Zheng, Influence of pore size on discharge capacity in Li-air batteries with hierarchically macroporous carbon nanotube foams as cathodes, J. Electrochem. Soc. 165 (2018) A2833–A2839, https://doi.org/10.1149/2.1141811jes.
[17] F. Wu, J.T. Lee, A. Magasinski, H. Kim, G. Yushin, Solution-based processing of graphene-Li2S composite cathodes for lithium-ion and lithium-sulfur batteries, Part. Part. Syst. Char. 31 (2014) 639–644, https://doi.org/10.1002/ppsc.201300358.
[18] S. Chen, Y. Gao, Z. Yu, M.L. Gordin, J. Song, D. Wang, High capacity of lithium-sulfur batteries at low electrolyte/sulfur ratio enabled by an organosulfide containing electrolyte, Nanomater. Energy 31 (2017) 418–423, https://doi.org/10.1016/j.nanoen.2016.11.057.
[19] N. Ding, S.W. Chien, T.S.A. Hor, Z. Liu, Y. Zong, Key parameters in design of lithium sulfur batteries, J. Power Sources 269 (2014) 111–116, https://doi.org/10.1016/j.jpowsour.2014.07.008.
[20] K. Sun, H. Liu, H. Gan, Cathode loading effect on sulfur utilization in lithium–sulfur battery, J. Electrochem. Energy Convers. Storage. 13 (2016) 021002, https://doi.org/10.1115/1.4034738.
[21] P. Andrei, C. Shen, J.P. Zheng, Theoretical and experimental analysis of precipitation and solubility effects in lithium-sulfur batteries, Electrochim. Acta 284 (2018) 469–484, https://doi.org/10.1016/j.electacta.2018.07.045.
[22] M. Li, Y. Zhang, Z. Bai, W.W. Liu, T. Liu, J. Gim, G. Jiang, Y. Yuan, D. Luo, K. Feng, R.S. Yassar, X. Wang, Z. Chen, J. Lu, A lithium-sulfur battery using a 2D current collector architecture with a large-sized sulfur host operated under high areal loading and low E/S ratio, Adv. Mater. 30 (2018) 1804271, https://doi.org/10.1002/adma.201804271.
[23] B. Li, J. Zheng, H. Zhang, L. Jin, D. Yang, H. Lv, C. Shen, A. Shellikeri, Y. Zheng, R. Gong, J.P. Zheng, C. Zhang, Electrode materials, electrolytes, and challenges in nonaqueous lithium-ion capacitors, Adv. Mater. 1705670 (2018) 1705670, https://doi.org/10.1002/adma.201705670.
[24] Q. Pang, J. Tang, H. Huang, X. Liang, C. Hart, K.C. Tam, L.F. Nazar, A nitrogen and sulfur dual-doped carbon derived from Polyrhodanine@Cellulose for advanced lithium-sulfur batteries, Adv. Mater. 27 (2015) 6021–6028, https://doi.org/10.1002/adma.201502467.
[25] G. Li, X. Wang, M.H. Seo, M. Li, L. Ma, Y. Yuan, T. Wu, A. Yu, S. Wang, J. Lu, Z. Chen, Chemisorption of polysulfides through redox reactions with organic molecules for lithium-sulfur batteries, Nat. Commun. 9 (2018) 1–10, https://doi.org/10.1038/s41467-018-03116-z.
[26] W. Guo, Y. Fu, A perspective on energy densities of rechargeable Li-S batteries and alternative sulfur-based cathode materials, Energy Environ. Mater. 1 (2018) 20–27, https://doi.org/10.1002/eem2.12003.
[27] C. Li, H. Zhang, L. Otaegui, G. Singh, M. Armand, L.M. Rodriguez-Martinez, Estimation of energy density of Li-S batteries with liquid and solid electrolytes, J. Power Sources 326 (2016) 1–5, https://doi.org/10.1016/j.jpowsour.2016.06.109.
[28] J. Gao, H.D. Abruña, Key parameters governing the energy density of rechargeable Li/S batteries, J. Phys. Chem. Lett. 5 (2014) 882–885, https://doi.org/10.1021/jz5001819.
[29] M. Wild, L. O'Neill, T. Zhang, R. Purkayastha, G. Minton, M. Marinescu, G.J. Offer, Lithium sulfur batteries, a mechanistic review, Energy Environ. Sci. 8 (2015) 3477–3494, https://doi.org/10.1039/C5EE01388G.
[30] S. Drvarič Talian, J. Moškon, R. Dominko, M. Gaberšček, Reactivity and diffusivity of Li polysulfides: a fundamental study using impedance spectroscopy, ACS Appl. Mater. Interfaces 9 (2017) 29760–29770, https://doi.org/10.1021/acsami.7b08317.
[31] S.H. Chung, P. Han, A. Manthiram, A polysulfide-trapping interface for electrochemically stable sulfur cathode development, ACS Appl. Mater. Interfaces 8 (2016) 4709–4717, https://doi.org/10.1021/acsami.5b12012.
[32] V.S. Kolosnitsyn, E.V. Kuzmina, E.V. Karaseva, S.E. Mochalov, A study of the electrochemical processes in lithium-sulphur cells by impedance spectroscopy, J. Power Sources 196 (2011) 1478–1482, https://doi.org/10.1016/j.jpowsour.2010.08.105.
[33] C.-F. Chen, A. Mistry, P.P. Mukherjee, Probing impedance and microstructure evolution in lithium-sulfur battery electrodes, J. Phys. Chem. C (2017), https://doi.org/10.1021/acs.jpcc.7b07245 acs.jpcc.7b07245.
[34] Z. Yang, S. Wang, K. Dong, Y. Dai, X. Lei, Electrochemical characterization of sulfur with low depth of charge/discharge in lithium sulfur batteries, Electrochim. Acta 187 (2016) 629–635, https://doi.org/10.1016/j.electacta.2015.11.116.
[35] N.A. Canas, K. Hirose, B. Pascucci, N. Wagner, K.A. Friedrich, R. Hiesgen, Investigations of lithium-sulfur batteries using electrochemical impedance spectroscopy, Electrochim. Acta 97 (2013) 42–51, https://doi.org/10.1016/j.electacta.2013.02.101.
[36] L. Yuan, X. Qiu, L. Chen, W. Zhu, New insight into the discharge process of sulfur cathode by electrochemical impedance spectroscopy, J. Power Sources 189 (2009) 127–132, https://doi.org/10.1016/j.jpowsour.2008.10.033.
[37] K. Yang, L. Zhong, Y. Mo, R. Wen, M. Xiao, D. Han, S. Wang, Y. Meng, A functional separator coated with sulfonated poly(styrene-ethylene-butylene-styrene) to synergistically enhance the electrochemical performance and anti-self-discharge behavior of Li–S batteries, ACS Appl. Energy Mater. (2018) 8b00275, https://doi.org/10.1021/acsaem.8b00275 acsaem.
[38] Z. Li, S. Deng, H. Li, H. Ke, D. Zeng, Y. Zhang, Y. Sun, H. Cheng, Explore the influence of coverage percentage of sulfur electrode on the cycle performance of lithium-sulfur batteries, J. Power Sources 347 (2017) 238–246, https://doi.org/10.1016/j.jpowsour.2017.02.069.
[39] Y.-S. Su, Y. Fu, T. Cochell, A. Manthiram, A strategic approach to recharging lithium-sulphur batteries for long cycle life, Nat. Commun. 4 (2013) 2985, https://doi.org/10.1038/ncomms3985.
[40] S. Choudhury, B. Krüner, P. Massuti-Ballester, A. Tolosa, C. Prehal, I. Grobelsek, O. Paris, L. Borchardt, V. Presser, Microporous novolac-derived carbon beads/sulfur hybrid cathode for lithium-sulfur batteries, J. Power Sources 357 (2017) 198–208, https://doi.org/10.1016/j.jpowsour.2017.05.005.
[41] M. Cuisinier, P.-E. Cabelguen, B.D. Adams, A. Garsuch, M. Balasubramanian, L.F. Nazar, Unique behaviour of nonsolvents for polysulphides in lithium-sulphur batteries, Energy Environ. Sci. 7 (2014) 2697, https://doi.org/10.1039/C4EE00372A.
[42] L. Jin, G. Li, B. Liu, Z. Li, J. Zheng, J.P. Zheng, A novel strategy for high-stability lithium sulfur batteries by in situ formation of polysulfide adsorptive-blocking layer, J. Power Sources 355 (2017) 147–153, https://doi.org/10.1016/j.jpowsour.2017.04.059.
[43] W. Yang, W. Yang, A. Song, L. Gao, G. Sun, G. Shao, Pyrrole as a promising electrolyte additive to trap polysulfides for lithium-sulfur batteries, J. Power Sources 348 (2017) 175–182, https://doi.org/10.1016/j.jpowsour.2017.03.008.
[44] Y.X. Ren, T.S. Zhao, M. Liu, Y.K. Zeng, H.R. Jiang, A self-cleaning Li-S battery enabled by a bifunctional redox mediator, J. Power Sources 361 (2017) 203–210, https://doi.org/10.1016/j.jpowsour.2017.06.083.
[45] H.J. Peng, J.Q. Huang, X.Y. Liu, X.B. Cheng, W.T. Xu, C.Z. Zhao, F. Wei, Q. Zhang, Healing high-loading sulfur electrodes with unprecedented long cycling life: spatial heterogeneity control, J. Am. Chem. Soc. 139 (2017) 8458–8466, https://doi.org/10.1021/jacs.6b12358.
[46] C.Y. Fan, S.Y. Liu, H.H. Li, Y.H. Shi, H.F.H.C. Wang, H.F.H.C. Wang, H.Z. Sun, X.L. Wu, J.P. Zhang, Synergistic mediation of sulfur conversion in lithium-sulfur batteries by a Gerber tree-like interlayer with multiple components, J. Mater. Chem. A. 5 (2017) 11255–11262, https://doi.org/10.1039/c7ta02231j.
[47] Z. Cui, C. Zu, W. Zhou, A. Manthiram, J.B. Goodenough, Mesoporous titanium nitride-enabled highly stable lithium-sulfur batteries, Adv. Mater. (2016) 6926–6931, https://doi.org/10.1002/adma.201601382.